Article

Novel Configuration for a Multistage Flash-Mixer Desalination System

Sergio F. Mussati, Pio A. Aguirre, and Nicols J. Scenna

Ind. Eng. Chem. Res., **2003**, 42 (20), 4828-4839• DOI: 10.1021/ie020318v • Publication Date (Web): 22 August 2003

Novel Configuration for a Multistage Flash-Mixer Desalination System

Sergio F. Mussati,† Pio A. Aguirre,* and Nicolás J. Scenna‡

INGAR, Instituto de Desarrollo y Diseño, Universidad Nacional del Litoral, Avellaneda 3657, 3000 Santa Fe, Argentina

In this paper a systematic procedure for the synthesis and design of multistage flash-mixer desalination processes is presented. The process configuration, geometric design, and optimal operating conditions are determined by minimizing the total annualized cost for a given water production. Different possible arrangements for the desaltor are embedded in a superstructure. The multistage flash-mixer system is rigorously modeled considering the most important aspects of the real process. The resolution procedure involves two phases. First, a simplified model is solved in a preprocessing phase providing the initial values and bounds, and then from these values the rigorous model is easily solved. For the simplified model resolution in the preprocessing phase, there is no need for supplying and tuning external parameters for initialization. The preprocessing phase increases the robustness of the optimization algorithm. A new configuration of the multistage flash-mixer system system resulted. This new structure differs from the conventional one because it considers distillate extraction and a new allocation of the blowdown brine (generally placed at the last stage). Different study cases are presented to illustrate the methodology robustness and computational performance.

1. Introduction

1.1. Previous Works. Chemical process synthesis is a steadily developing area in process engineering. There exist a large number of papers and reviews on this area.[1]

However, in the literature related to seawater desalination processes, there are no papers aimed at the simultaneous optimization of the structure and operating conditions to approach the optimal synthesis and design problem. The generations of new structures resulted from the creative judgment of the designer but were not supported by a conceptual and methodological background.

In the last years, many studies have been presented about the multistage flash (MSF) desalination system. Nevertheless, no relevant improvements on the flow pattern distribution have been achieved to improve the thermodynamic efficiency and/or the economy of the process.[2]

Even though some works related to the desalination process synthesis have been published, they do not present a systematic methodology for achieving an optimal structure.[2−4] Instead, the analysis is carried out for each fixed structure, and then the structures are compared.[4]

The aim of this work is to present a synthesis strategy for the multistage flash-mixer (MSF-M) system. Both a new rigorous stage-by-stage model and a process superstructure are developed. The proposed superstructure considers the feed allocation, the product (distillate) flow pattern, the number of stages, and the operating conditions as variables.

The proposed methodology first considers the solution of a simplified model (a preprocessing phase) to determine initial values and some critical lower bounds. The latter are used to solve the rigorous model. The advantages of this method are (a) the algorithm is robust; (b) the optimal solutions of the simplified model are easily obtained, and the global optimality is demonstrated (this condition was investigated by comparing the solutions achieved using a global optimization deterministic algorithm[5] to those achieved using CONOPT[6]); and (c) feed and blowdown stream allocations can be estimated.

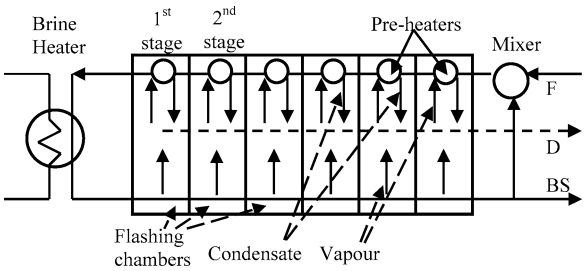

Figure 1. Flowsheet for the MSF-M evaporation system.

1.2. Process Description. MSF-M plants are used to produce large quantities of potable water. Figure 1 depicts the MSF-M desalination process.

This process is very similar to the multi-effect evaporation (MEE), except for the difference in the way in which evaporation is produced. In MEE systems, the driving force is the temperature gradient between the vapor coming from the previous effect and the brine, while in the MSF-M system, the driving force for evaporation is the pressure gradient established in each stage, causing successive flashings of the circulating fluid.

MSF-M Plants. Figure 1 briefly illustrates the process. The evaporator is divided into stages; each stage contains a seawater preheater, a brine flashing chamber, a demister, and a distillate collector. A typical flashing stage is shown in Figure 2.

The seawater feed (F) containing dissolved noncon-

* To whom correspondence should be addressed. Tel.: +54 342 455 5229. Fax: +54 342 455 3439. E-mail: paguir@ceride.gov.ar.

†E-mail: mussati@ceride.gov.ar.

‡ E-mail: nscenna@ceride.gov.ar.

10.1021/ie020318v CCC: $25.00
Published on Web 08/22/2003

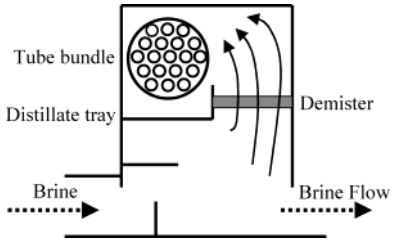

Figure 2. Scheme of a typical flashing stage.

densable gases is deaerated to minimize gas concentrations. A suitable integral deaerator working under vacuum shall be provided to remove carbon dioxide, air, and other noncondensable elements from the seawater. The deaerator design shall ensure that the feedwater contains less than 100 ppb of dissolved oxygen (O_2) and shall practically eliminate carbon dioxide (CO_2). The level of dissolved oxygen is further reduced by the injection of sodium bisulfate in order to ensure minimum corrosion levels in the plant. This introduces a pretreatment cost.

The seawater feed (F) previously treated with antiscalent chemicals after screening is heated as it flows in series in the condenser tubes at each stage and the brine heater, being heated to a temperature greater than the saturation temperature at the final stage. It then flows into the first stage inlet box (flash chamber), and it is evenly distributed across the width of the evaporator. It enters each stage through an orifice and a weir system that control its flow rate and the flashing characteristics. Then, the flashed vapor flows first through a demister, which removes any entrained brine, and then over a condenser that condenses it. The vapor release velocity from the flashing brine surfaces shall be as low as possible to minimize brine carryover. The maximum vapor release velocity shall not exceed 8−9 m/s and is ensured by providing an adequate cross-sectional area (length and width) for the flashing chamber.

The condensate, referred to as the distillate (D), is collected in a distillate collector. The seawater, now referred to as brine because its salinity has increased, then flows through the evaporator stages in turn, releasing flashed vapor at each stage in the same way. The brine (BS) is rejected from the last stage evaporator by a brine blowdown pump to the sea. Part of this stream is recycled and mixed with the feed to enter the preheater tubes as previously described.

The distillate accumulated in each stage passes through the transfer system into the next lower temperature stage, where a proportion is similarly flashed to the brine. This vapor flows over the stage condenser together with the vapor flashed from the brine, and it is condensed and transferred to the next stage. The distillate accumulates as it flows through stages and is discharged from the last stage to a product water tank by the distillate pump.

It is desirable to raise the brine temperature at the inlet of the first chamber to the maximum possible value in order to attain higher plant efficiency and a reduction in capital cost. However, the tendency to scale formation increases too. With polyphosphate treatment, the maximum brine temperature leaving the brine heater is limited to 90.5 °C, which represents the safe limit for operation. Higher temperatures cause polyphosphate hydrolysis, leading to a loss of effectiveness and sludge formation. If special polymer additives are used, the maximum brine temperature could be raised to 112−115 °C.

The above description corresponds to conventional MSF-M desalination systems. In this work, using mathematical programming, we propose a superstructure for this process considering simultaneously different stream flow patterns (distillate, waste brine, and feed).

2. Problem Definition

The proposed superstructure is illustrated in Figure 3. It takes into account the number of stages and the stream patterns of the blowdown, recycle, and distillate.

The objective is to determine the optimal process design and operating conditions minimizing the total annual cost. The water production rate, maximum operation temperature, seawater temperature and composition, and cost data are assumed as given.

3. Rigorous Model

The development of a rigorous model with a high detail level considering the most important aspects of the process is needed. In this section, a rigorous nonlinear programming (NLP) model based on the superstructure for a MSF-M desalination system is presented.

The model is derived by considering rigorous material, momentum, and energy balances for each stage. The index j denotes the stage number. The optimal number of stages (NS_{optim}) is obtained as a result of solving the model superstructure, and the maximum value adopted is 40 stages. This value is selected considering the operating conditions of the evaporator in order to guarantee a stable operation.[7] A minimal pressure difference between adjacent stages should be kept to ensure a stable operation. A value higher than 40 could cause operability problems due to negligible driving forces for brine and distillate flows.

A flashing unit is modeled considering a principal chamber, a secondary chamber, a demister, and a preheater (Figure 2).

3.1. Model Assumptions. The rigorous model is derived on the basis of the following hypothesis:

(i) The preheater heat-transfer area and the surface area of each flashing chamber are considered in the objective function. The main brine heat-transfer area is not considered because it is included in the utility system.

(ii) The system is well insulated.

(iii) The dependence of the heat capacity (C_p), boiling point elevation (BPE), and latent heat of evaporation (λ_v) on the temperature and concentration is considered by rigorous correlations.

(iv) The dependence of the overall heat-transfer coefficient (U) on the brine velocity, temperature, and tube diameter is considered.[8]

(v) The nonequilibrium allowance (NEA) is taken into account according to the correlation developed by Helal et al.[9] It represents a measure of the flash thermal efficiency and depends on the stage flashing temperature, the brine level inside the flashing chamber, and the brine flow rate per unit of stage width.

(vi) Hydraulic correlations given by ref 3 are adopted. These equations describe the interstage flow rate of the flashing brine. The transport of the distillate and flashing brine streams depends on both the stage vapor

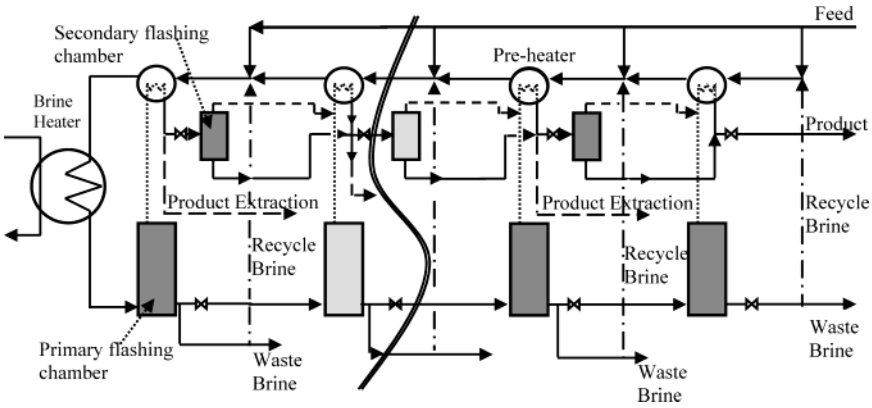

Figure 3. Superstructure for the MSF-M system.

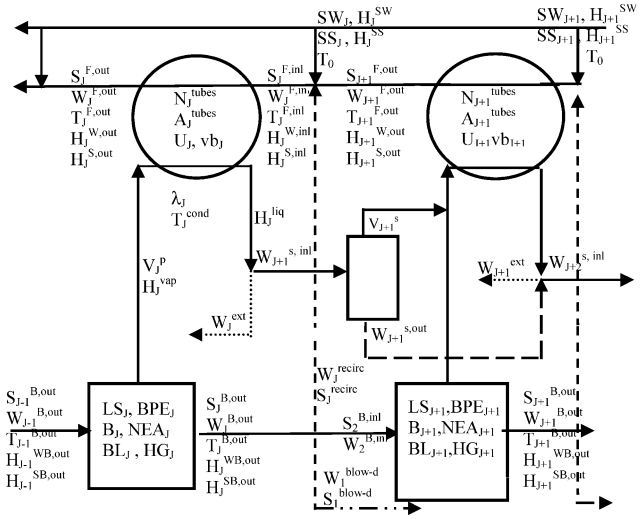

Figure 4. Schematic representation of the *j*th stage.

pressure and the liquid level in two adjacent chambers. The orifice design is also taken into account.

(vii) The preheater tube configuration is arranged perpendicularly to the brine flow.

(viii) A stage geometric design (length, width, and height) is considered.

(ix) Noncondensable effects are neglected.

(x) Recycle streams are considered (MSF-M system).

(xi) Different allocations of distillate extraction, feed, and brine withdrawal are considered as model variables.

Figure 4 depicts a generic *j*th stage and the main process variables.

3.2. Mathematical Model. Objective Function. The objective is to minimize the total annual cost, which is mainly composed of the operating costs and investments. The former include the steam utility, seawater pretreatment, and pumping costs (SC, PFC, and PC, respectively). The investment cost includes the preheater area (AC) and the flashing chambers including its related pipelines (NC).

The objective function is defined as follows:

$$\mathrm{TAC} = \mathrm{SC} + \mathrm{PFC} + \mathrm{PC} + \mathrm{AC} + \mathrm{NC}$$

If pumping costs PC are neglected, the objective function becomes

$$\mathrm{TAC} = C_{\mathrm{Q}}Q^{\mathrm{Des}} + C_{\text{treatment}}\mathrm{Feed} + C_{\text{tubing area}}A_{\text{tubing}} + C_{\text{stage area}}A_{\text{stage}}$$

where C_{Q}, $C_{\text{tubing area}}$, $C_{\text{stage area}}$, and $C_{\text{treatment}}$ are the hot utility unit cost, unit cost of the heat-transfer area, unit cost of the chamber superficial area, and pretreatment unit cost, respectively.

Depending on the process conditions (composition, flow rates, and temperature), different materials may be required for different equipment parts. The heat-transfer area unit cost and the stage area unit cost are related by the "weight" factor F. This factor F takes into account resistance to corrosion, tendencies to form scale, and mechanical strength that depends on the material used for the chamber construction and its geometry. Indeed, it also includes chamber instrumentations, roller expansion, drilling of the tubes, and welding. Typical values of F estimated in this way usually range between 10 and 40.[10] According to this, the objective function is

$$\mathrm{TAC} = C_{\mathrm{Q}}Q^{\mathrm{Des}} + C_{\text{treatment}}\mathrm{Feed} + C_{\text{tubing area}}(A_{\text{tubing}} + FA_{\text{stage}})$$

Constraints for the problem are as follows.

Mass conservation equation for each primary stage

$$W_j^{\mathrm{B,inl}} - W_j^{\mathrm{B,out}} - V_j^{\mathrm{p}} = 0 \qquad j = 1, ..., \mathrm{NS}, ..., 40 \qquad (1)$$

$$S_j^{\mathrm{B,inl}} - S_j^{\mathrm{B,out}} = 0 \qquad j = 1, ..., \mathrm{NS}, ..., 40 \qquad (2)$$

Energy balance

$$W_j^{\mathrm{B,inl}} H_j^{\mathrm{WB,inl}} + S_j^{\mathrm{B,inl}} H_j^{\mathrm{SB,inl}} - ... - W_j^{\mathrm{B,out}} H_j^{\mathrm{WB,out}} - V_j^{\mathrm{p}} H_j^{\mathrm{vap}} - S_j^{\mathrm{B,out}} H_j^{\mathrm{SB,out}} = 0 \qquad j = 1, ..., \mathrm{NS}, ..., 40 \qquad (3)$$

Mass and energy balances for each secondary stage

$$W_j^{\mathrm{s,inl}} - W_j^{\mathrm{s,out}} - V_j^{\mathrm{s}} = 0 \qquad j = 1, ..., \mathrm{NS}, ..., 40 \qquad (4)$$

$$W_j^{\mathrm{s,out}} + V_j^{\mathrm{s}} + V_j^{\mathrm{p}} - W_{j+1}^{\mathrm{s,inl}} - W_j^{\mathrm{ext}} = 0 \qquad j = 1, ..., \mathrm{NS}, ..., 39 \qquad (5)$$

$$W_j^{\mathrm{s,out}} + V_j^{\mathrm{s}} + V_j^{\mathrm{p}} - W_j^{\mathrm{ext}} = 0 \qquad j = 40 \qquad (6)$$

$$W_j^{s,inl} H_{j-1}^{liq} - W_j^{s,out} H_j^{liq} - V_j^{s} H_j^{vap} = 0 \qquad j = 2, ..., NS, ..., 40 \quad (7)$$

$$W_j^{s,out} + V_j^{s} = 0 \qquad j = 1 \quad (8)$$

In each preheater, the mass balance is

$$W_{j+1}^{F,out} + W_j^{recirc} + SW_j - W_j^{F,inl} = 0 \qquad j = 1, ..., NS, ..., 39 \quad (9)$$

$$W_j^{recirc} + SW_j - W_j^{F,inl} = 0 \qquad j = 40 \quad (10)$$

$$S_{j+1}^{F,out} + S_j^{recirc} + SS_j - S_j^{F,inl} = 0 \qquad j = 1, ..., NS, ..., 40 \quad (11)$$

$$S_j^{recirc} + SS_j - S_j^{F,inl} = 0 \qquad j = 40 \quad (12)$$

$$X_{feed} = \frac{SS_j}{SS_j + SW_j} \qquad j = 1, ..., NS, ..., 40 \quad (13)$$

$$W_j^{F,inl} - W_j^{F,out} = 0 \qquad j = 1, ..., NS, ..., 40 \quad (14)$$

$$S_j^{F,inl} - S_j^{F,out} = 0 \qquad j = 1, ..., NS, ..., 40 \quad (15)$$

$$W_j^{F,out} - W_j^{B,inl} = 0 \qquad j = 1 \quad (16)$$

$$S_j^{F,out} - S_j^{B,inl} = 0 \qquad j = 1 \quad (17)$$

The energy balance is

$$(V_j^{p} + V_j^{s})\lambda_j - W_j^{F,out}(H_j^{W,out} - H_j^{W,inl}) - ... - S_j^{F,out} (H_j^{S,out} - H_j^{S,inl}) = 0 \qquad j = 1, ..., NS, ..., 40 \quad (18)$$

$$W_j^{F,inl} H_j^{W,inl} - W_j^{recirc} H_j^{W,out} - SW_j H_j^{w,feed} - ... - W_{j+1}^{F,out} H_{j+1}^{W,out} + S_j^{F,inl} H_j^{S,inl} - S_j^{recirc} H_j^{S,out} - ... - SS_j H_j^{s,feed} - S_{j+1}^{F,out} H_{j+1}^{S,out} = 0 \qquad j = 1, ..., NS, ..., 40 \quad (19)$$

$$W_j^{F,inl} H_j^{W,inl} - W_j^{recirc} H_j^{W,out} - SW_j H_j^{w,feed} + ... + S_j^{F,inl} H_j^{S,inl} - S_j^{recirc} H_j^{S,out} - SS_j H_j^{s,feed} = 0 \qquad j = 40 \quad (20)$$

Relations incorporated due to brine recirculation are the following:

Mass balance

$$W_j^{B,out} - W_j^{blow-d} - W_j^{recirc} - W_{j+1}^{B,inl} = 0 \qquad j = 1, ..., NS, ..., 40 \quad (21)$$

$$W_j^{B,out} - W_j^{blow-d} - W_j^{recirc} = 0 \qquad j = 40 \quad (22)$$

$$S_j^{B,out} - S_j^{blow-d} - S_j^{recirc} - S_{j+1}^{B,inl} = 0 \qquad j = 1, ..., NS, ..., 39 \quad (23)$$

$$S_j^{B,out} - S_j^{blow-d} - S_j^{recirc} = 0 \qquad j = 40 \quad (24)$$

$$X_j^{out} = \frac{S_j^{B,out}}{S_j^{B,out} + W_j^{B,out}} \qquad j = 1, ..., NS, ..., 40 \quad (25)$$

$$X_j^{out} = \frac{S_j^{recirc}}{S_j^{recirc} + W_j^{recirc}} \qquad j = 1, ..., NS, ..., 40 \quad (26)$$

$$X_j^{out} = \frac{S_j^{blow-d}}{S_j^{blow-d} + W_j^{blow-d}} \qquad j = 1, ..., NS, ..., 40 \quad (27)$$

Energy balance

$$Q^{Des} = W_j^{F,out}(H_{w,max} - H_j^{W,out}) + S_j^{F,out}(H_{s,max} - H_j^{S,out}) \qquad j = 1 \quad (28)$$

Design equations are the following:

Heat-exchange area for each stage:

$$(V_j^{p} + V_j^{s})\lambda_j = U_j A_j^{tubes} \Delta tml_j \qquad j = 1, ..., NS, ..., 40 \quad (29)$$

where

$$\Delta tml_j = \left[\frac{(T_j^{cond} - T_j^{F,inl})(T_j^{cond} - T_j^{F,out})[(T_j^{cond} - T_j^{F,inl}) + (T_j^{cond} - T_j^{F,out})]}{2}\right]^{\frac{1}{3}} \qquad j = 1, ..., NS, ..., 40 \quad (30)$$

Vapor velocity

$$LS_j B_j = \frac{V_j^{p}}{Vel_{vap}^{j} \rho_{vap}^{j}} \qquad j = 1, ..., NS, ..., 40 \quad (31)$$

From the momentum balance, the gate height is calculated:

$$W_j^{B,out} + S_j^{B,out} = \rho_{brine}^{j} C_d B_j HG_j \sqrt{2g(BL_j - BL_{j+1}) + \frac{(P_j^{vap} - P_{j+1}^{vap})}{\rho_{brine}^{j}}} \qquad j = 1, ..., NS, ..., 39 \quad (32)$$

The number of tubes for each preheater is

$$N_j^{tubes} = \frac{A_j^{tubes}}{2\pi B_j} \qquad j = 1, ..., NS, ..., 40 \quad (33)$$

From a mass balance, the total number of tubes is

$$N_j^{tubes} = \frac{4(W_j^{F,out} + S_j^{F,out})}{\pi d_i^{\,2} \rho_{brine}^{j} Vb_j} \qquad j = 1, ..., NS, ..., 40 \quad (34)$$

For tubes in an equilateral triangular pitch arrangement, the number of rows of tubes N^J can be predicted from the following equation:

$$N^J = 0.481(N_j^{tubes})^{0.505} \qquad j = 1, ..., NS, ..., 40 \quad (35)$$

The shell diameter is related to the number of rows of tubes N^J and pitch P_t by

$$N^J = \frac{D_j^S}{\sqrt{2}P_t} \qquad j = 1, ..., NS, ..., 40 \qquad (36)$$

The chamber superficial stage area is

$$A_j^{stage} = 2LS_jB_j + 2(HG_j + D_j^S)LS_j + B_j(HG_j + D_j^S) \qquad j = 1, ..., NS, ..., 40 \quad (37)$$

Feasibility temperature constraints (decreasing temperature through stages)

$$T_{Max} \geq T_j^{B,out} \qquad j = 1 \qquad (38)$$

$$T_j^{B,out} \geq T_{j+1}^{B,out} \qquad j = 1, ..., NS, ..., 39 \qquad (39)$$

$$T_j^{F,out} \geq T_j^{F,inl} \qquad j = 1, ..., NS, ..., 40 \qquad (40)$$

$$T_j^{cond} \geq T_j^{F,out} \qquad j = 1, ..., NS, ..., 40 \qquad (41)$$

Physical−chemical properties (nonlineal functions)

$$U_j = f(vb_j, T_j^{F,out}, T_j^{cond}, TD, FF) \qquad j = 1, ..., NS, ..., 40 \quad (42)$$

$$BPE_j = f(T_j^{B,out}, X_j^{out}) \qquad j = 1, ..., NS, ..., 40 \qquad (43)$$

$$NEA_j = f\left[BL_j, (T_j^{B,inl} - T_j^{B,out}), T_j^{cond}, \frac{W_j^{B,inl}}{B_j}\right] \qquad j = 2, ..., NS, ..., 40 \quad (44)$$

$$NEA_j = f\left[BL_j, (T_{Max} - T_j^{B,out}), T_j^{cond}, \frac{W_j^{B,inl}}{B_j}\right] \qquad j = 1 \quad (45)$$

$$H_j^{W,out} = f(T_j^{F,out}) \qquad j = 1, ..., NS, ..., 40 \qquad (46)$$

$$H_j^{W,inl} = f(T_j^{F,inl}) \qquad j = 1, ..., NS, ..., 40 \qquad (47)$$

$$H_j^{S,out} = f(T_j^{F,out}) \qquad j = 1, ..., NS, ..., 40 \qquad (48)$$

$$H_j^{S,inl} = f(T_j^{F,inl}) \qquad j = 1, ..., NS, ..., 40 \qquad (49)$$

$$H_j^{vap} = f(T_j^{cond}) \qquad j = 1, ..., NS, ..., 40 \qquad (50)$$

$$H_j^{liq} = f(T_j^{cond}) \qquad j = 1, ..., NS, ..., 40 \qquad (51)$$

$$H_j^{WB,inl} = f(T_j^{B,inl}) \qquad j = 1, ..., NS, ..., 40 \qquad (52)$$

$$H_j^{SB,inl} = f(T_j^{B,inl}) \qquad j = 1, ..., NS, ..., 40 \qquad (53)$$

$$P_j^{vap} = f(T_j^{cond}) \qquad j = 1, ..., NS, ..., 40 \qquad (54)$$

Correlations used are listed in Appendix I.

The complete steady-state model for the MSF system is described by eqs 1−54, which are the constraints for the optimization problem.

The equation system is highly nonlinear, making it difficult to achieve the optimal solution. The two following phenomena are well-known in large-scale NLP problems: (a) infeasible solutions are obtained if the initial values are far away from the feasible region; (b) local solutions are achieved in the neighborhood of the first feasible solution instead of the global one. It will be shown that setting both upper and lower bounds on a few critical model variables and using appropriate initial values (i.e., the value of all of the variables at "iteration zero") is a critical aspect, especially to guarantee feasibility and convergence and to determine, if possible, the global optimum.

In this work, both mentioned aspects are approached and taken into account in the proposed methodology. Convergence of the rigorous model is guaranteed by a "preprocessing phase" that allows one to obtain a feasible solution with only a few iterations. The preprocessing phase uses an optimal solution obtained using the simplified model (section 4). This solution is used as the initialization to solve the rigorous model by increasing the robustness of the optimization algorithm.

The model was implemented in GAMS (General Algebraic Modeling System)[11] and solved using the generalized reduced gradient algorithm CONOPT 2.041.

4. Problem Solving Methodology

As previously mentioned, the preprocessing phase (the first one of the procedure) involves a simplified model and the second one considers the rigorous optimization model (Figure 5).

Before the methodologyis described, the following section presents a brief discussion on some aspects of the simplified model that will be used in the procedure.

Simplified Model. Scenna[13] developed a thermodynamic-based model for the MSF process in order to determine the optimal parameters for preliminary design. The model was derived by extending the heat-exchange network synthesis theory proposed by Linnhoff and Flower.[12] A summarized version of the mathematical model that relates the main operating variables can be found in Appendix II (for more details, see ref 13). The model includes inherently nonlinear and nonconvex constraints.

Marcovecchio and Mussati[14] applied the global optimization approach developed in ref 5 to solve this simplified model obtaining the global solution. The same solution is obtained using local solver CONOPT.[15] Moreover, for each possible range of the problem parameters (maximum temperature T_{max}, seawater temperature T_0, initial composition C_p, and λ) the global optimal solution is always obtained by departing from a wide range of positive initial values. This aspect is very important because we can always obtain the optimal solution without computational difficulties and

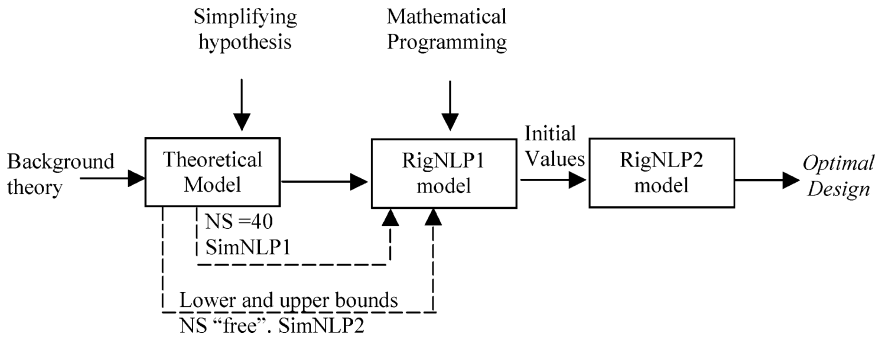

Figure 5. Procedure to solve the NLP rigorous model.

Table 1. Parameter Values

C_A [\$/m^2]	C_{Qdes} [\$/10^6 Btu]	C_{Teat} [\$/kg·year]	CRF [year^{-1}]	T_{Max} [K]	T_{SW} [K]	X_0 [ppm]	Prod [tons/h]
50	0.40	0.001	0.082	393	298	45 000	1000

then use these solutions as an initial point to solve the rigorous models.

Preprocessing Phase. This phase requires SimNLP1 and SimNLP2 problems to be solved (see Figure 5). Both problems are based on the simplified model. The SimpNLP1 problem considers NS = 40, while in the SimNLP2 problem, NS is a variable.

As is shown in Figure 5, the initial values and the lower−upper bounds to be used in the RigNLP1 are calculated automatically from SimNLP1 and SimNLP2. These values guarantee the convergence of the RigNLP1 problem (rigorous optimization phase).

Let us remind everyone that the superstructure initialization must contemplate 40 stages. Indeed, it can be expected that the economic solution will show a lower number of stages. So, SimNLP1 is used to initialize the 40 stages of the RigNLP1. The SimNLP2 estimates the economic number of stages.

Solutions obtained from SimNLP1 and SimNLP2 problems are used in the following way:

(1) The optimal SimNLP1 solution is adopted as the initialization to solve RigNLP1. Some variables such as distillate extraction and liquid levels in flashing chambers are not directly available from the SimpNLP1 solution, but they are not critical for the algorithm.

(2) Then, the optimal SimNLP2 solution provides information about the approximated feed location (NS_{Opt}^{Simp}). According to this, NS_{Opt}^{Simp} predicts the stage candidates for the feed allocation.

The feed flow rate achieved by SimpNLP1 is distributed among stages (40) and $N_{Opt}^{Simp} - X$, where X represents a number of stages in order to consider any estimation error. Although optimal NS corresponding to the rigorous model is never lower than N_{Opt}^{Simp} for all studied cases, we adopt $X = 4$.

Because for real cases the optimal economic solution is characterized by NS lower than 40, certain variables (number of tubes, heat-transfer area, vapor produced, brine level, gate height, among others) should be zero in the optimal solution. So, there is an important aspect related to the correct elimination of stages in order to obtain the optimal solution without the need of a MINLP formulation. To achieve this efficiently, bounds on the feed flow rate in each stage are needed to solve the RigNLP1 model. These lower bounds are not arbitrary, and they are calculated by dividing the total feed flow rate obtained from SimNLP1 by the number of stages of candidates obtained from SimNLP2 ($N_{Opt}^{Simp} - X$).

Rigorous Optimization Phase. This phase requires RigNLP1 and RigNLP2 problems to be solved (see Figure 5). Both problems are based on the same rigorous model. The difference between both problems is that RigNLP1 considers lower bounds in the feed flow rate of each stage, while in the RigNLP2 problem, this value drops to zero.

Note that NS_{Opt}^{Simp} is not considered as a lower bound to solve RigNLP1 but as an approximated value to efficiently initialize the problem variables.

The solution obtained by RigNLP1 is used as the initialization to solve RigNLP2. The solution achieved from RigNLP2 indicates the optimal synthesis and design for the MSF process.

5. Study Cases

In this section, the algorithm results and the computational performance for two studied cases are presented. The operating parameters (seawater composition, maximum temperature, seawater temperature, and water production rate) of distiller no. 5 of Umm Al Nar East Plant, located in the Emirate of Abu Dhabi (UAE), have been adopted.

In example 1, the main characteristics related to a new structure for the MSF-M process are depicted. Also, advantages and disadvantages of the initialization procedures explained in the previous section are mentioned. On the other hand, to illustrate the flexibility and robustness of the methodology, various study cases are presented in example 2.

All study cases were solved using a Pentium III with 733 MHz and 256 MB RAM.

5.1. Study Case 1. Example 1. For the data given in Table 1, the object is to determine the system optimal configuration and operating conditions at minimum total annual cost according to our proposed methodology.

Figure 6 shows the values of the feed flow rate corresponding to each stage for both RigNLP1 and RigNLP2 problems.

It can be seen that, even in the solution of the RigNLP1 problem, the stage in which the feed will be allocated is easily identified (stage no. 29) while the feed flow rates in the remaining stages are in the lower bounds. These bounds are calculated by dividing the feed flow rate value obtained from SimNLP1 ($W = 3.6$ ton/h) by the potential feed-stage candidates ($40 - N_{Opt}^{Simp}$). N_{Opt}^{Simp}, as previously mentioned, is obtained

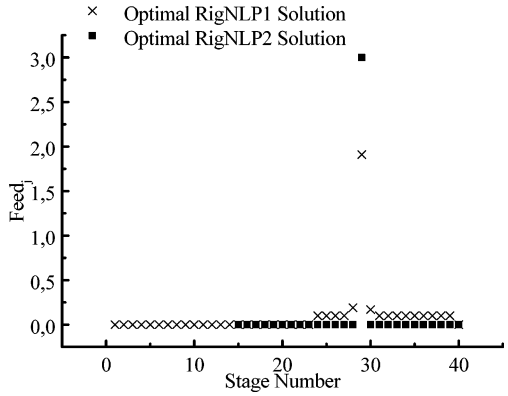

Figure 6. Feed distribution through the stages for RigNLP1 and RigNLP2 solutions.

from SimNLP2 (here $N_{Opt}^{Simp} = 27.3$). To impose these bounds on a robust and automatic program environment, it is necessary to define a dynamic set over $j = 1$ and 40 (a facility of GAMS that makes it possible to bound the feed flow rate of each stage as described above).

Therefore, by adopting this solution as an initial point and setting bounds to zero, the RigNLP2 problem is solved by obtaining the final solution.

Figure 7 shows the main characteristics of the obtained solution. This structure (hereafter named A) is different from the conventional one reported in the literature (hereafter named B). The comparison is on (a) product extraction, (b) allocation of a rejected stream, and (c) recycle stream distribution. In the following, each characteristic is discussed.

Product Extraction. In the new solution (Figure 7), the desaltor operates at stages $j = 1-21$ according to the MSF conventional theory or practice, while for $j = 22-29$, the produced vapor is totally extracted. Sommariva et al.[2] proposed a similar solution. A computer simulation has been carried out in order to investigate the effect of the extraction of the distillate from stage 1 and not allowing it to flow to the next stage. According to the authors, distillate extraction brings about both a higher performance ratio and greater water production than those reached with the conventional MSF desalination technique. This conclusion was supported by a simulation campaign fixing the configuration. In this paper, the same conclusion is pointed out but from an optimal economic synthesis point of view based on the proposed superstructure. Moreover, here both the amount (flow rates) and the distillate extraction allocations are exactly determined.

The effect of distillate extracting on the plant performance ratio (PR), which is defined as the ratio between the water production and heat consumption, is depicted in Figure 8. Typical PR values usually range between 5 and 10, depending on operating costs and investments. For PR = 5, the total area corresponding to structure A (with distillate extraction) is 7.24% lower than structure B (without extraction).

Distillate extraction is maintained as the optimal structure when the physical−chemical properties and other parameters are relaxed. For example, if the BPE effect, the chamber geometry, and recycle are not taken into account and the overall heat-transfer coefficient and evaporation latent heat are assumed as constant values, the same structure is obtained. That is, the effect of extracting distillate enhances the plant performance ratio. This can be easily explained by solving this "simpler" problem (based on these assumptions) and comparing the results for structure A to those for structure B, adopting nine stages for the process. The problem to be solved is

$$\text{Minimize} \sum_{j=1}^{9} A_j^{tubes}$$

given the feed flow rate (908.19 tons/h) and heat consumption (280 kcal/h).

Table 2 compares the solutions for both structures. Structure A produces 1000 tons/h requiring 8939.70 m^2 of heat-transfer area and extracts part of the distillate formed in stage nos. 3, 2, and 1. The distillate produced from stage no. 4 is extracted totally. The temperature of the blowdown stream is 325.83 K. On the other hand, structure B produces 957 tons/h requiring 8592.19 m^2 of heat-transfer area and a discharge temperature of 328.89 K. The total recovered heat (Q^{rec}) and heat consumption (Q^{Des}) in both structures are 582.72 and 280 Gcal/h, respectively. According to this, the total heat-transfer area of structure B is smaller than that of structure A because of a driving force increment, but its production is lower.

Although the total recovered heat is the same in both structures, the *ratio* between the recovered heat due to the vapor formed in stage j corresponding to the reflashing distillate produced in previous stages is different. This ratio is higher for structure A, increasing the performance ratio to structure B.

The difference between both solutions is the "reflash" operation of the distillate. Here, unlike classical problems of heat-exchange networks, the water production should be considered. There is a tradeoff among water production, heat recovered from reflashed distillate, and the heat-transfer area. As is shown in Table 2, distillate extraction is more attractive than the conventional configuration.

Table 2 also shows a significant decrease for structure A in both the logarithmic mean temperature (ΔT_{ml}) and heat-transfer area from stage $j = 3$, where the distillate extraction begins, whereas a flat profile is obtained for structure B.

Table 3 compares structures A and B for equal water production (1000 tons/h) and the same heat consumption (280 Gcal/h).

As is indicated in Table 3, to produce 1000 tons/h according to structure B, increments of 4.14% (9310.06 m^2) in the heat-transfer area and of 3.02% (936.32 tons/h) in the feed flow rate are required. According to this, for the same production, heat external consumption, and feed flow rate, the heat-transfer area for structure A is lower than that for structure B.

Finally, the same qualitative results were obtained for the first study case under analysis. For example, Figure 9 illustrates the logarithmic mean temperature distribution corresponding to structures A and B and for study case 1. Structure B presents a flat profile, whereas a decreasing profile is obtained for structure A from stage no. 22, where the distillate extraction begins.

Rejected Stream Allocation. Another different characteristic compared to the conventional structure is that the rejected stream W_{blow-d} is not located at the last stage. The optimal allocation of rejected stream is at stage no. 27, as can be seen in Figure 7. The allocation

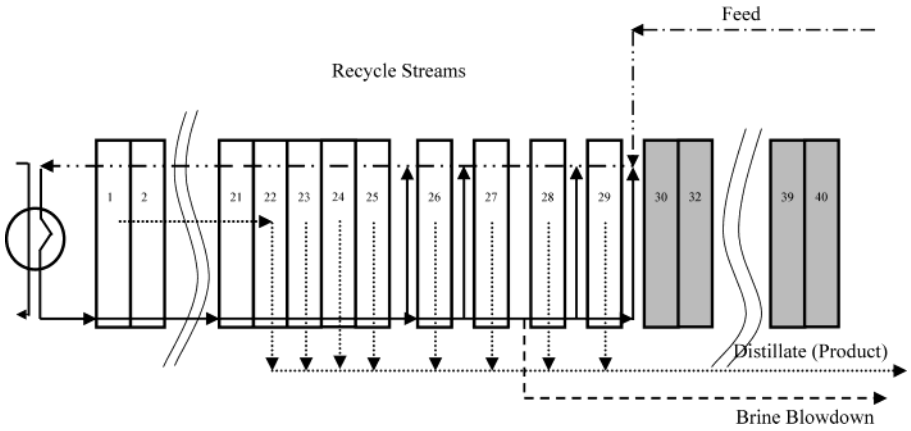

Figure 7. Main characteristics for the novel MSF-M configuration.

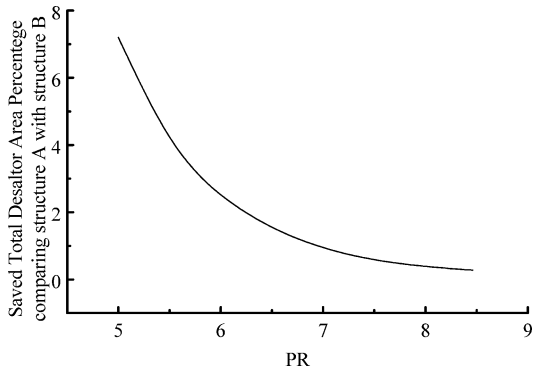

Figure 8. Comparison of the saved total desaltor area between the two different structures.

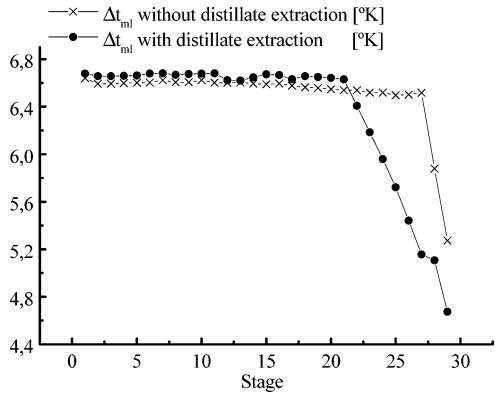

Figure 9. Logarithmic mean temperature distribution through the stages for study case 1 considering the extraction and nonextraction of distillate.

Table 2. Comparison of Structures A and B (Feed = 908.19 tons/h and NS = 9)

stage	structure	Q^{rec} [Gcal/h]	vapor prod [tons/h]	Δtml [K]	heat-transfer area [m^2]	extraction [tons/h]
1	A	62.14	107.15	27.31	910.14	0
	B	62.14	107.15	27.31	909.94	0
2	A	72.18	122.99	26.74	1079.73	0
	B	72.18	122.99	26.74	1079.36	0
3	A	72.18	121.31	26.77	1078.52	333.3
	B	72.18	121.31	26.77	1078.44	0
4	A	45.44	78.19	28.18	644.99	97.3
	B	45.44	75.32	28.37	640.60	0
5	A	62.14	107.15	26.85	925.73	107.15
	B	62.14	102.11	27.38	907.61	0
6	A	62.14	107.15	26.41	941.15	107.15
	B	62.14	100.91	27.38	907.81	0
7	A	62.14	107.15	25.87	960.80	107.15
	B	62.14	99.72	27.36	908.21	0
8	A	72.18	124.46	24.52	1177.48	124.46
	B	72.18	114.46	26.74	1079.64	0
9	A	72.18	124.46	23.63	1221.83	124.46
	B	72.18	112.89	26.72	1080.53	956.86
Total	A	582.72	1000		8939.70	1000
	B	582.72	956.86		8592.19	956.86

of these streams also produces lower values for logarithmic mean temperatures, as shown in Figure 9.

Recycle Stream Distribution. Finally, the recycle stream is not completely located at the last stage. The optimal allocation of the recycle stream is distributed along stage nos. 26−29 (Figure 7). Here, it is important to mention that we have not included the pumping cost in our objective function. Then, if we consider the pumping cost, which is composed by a fixed cost (associated to the pump) and variable cost depending on the brine flow rate, only one recycle stream is obtained (associated with stage no. 29), whereas the rest of the recycle streams corresponding to stage nos. 26−28 are eliminated.

Table 3. Comparison of Structures A and B (Water Production = 1000 tons/h and NS = 9)

stage	structure	Q^{rec} [Gcal/h]	vapor prod [tons/h]	Δtml [K]	heat-transfer area [m^2]	extraction [tons/h]
1	A	62.14	107.15	27.31	910.14	0
	B	62.14	107.15	26.51	937.96	0
2	A	72.18	122.99	26.74	1079.73	0
	B	72.18	123.04	25.94	1112.77	0
3	A	72.18	121.31	26.77	1078.52	333.3
	B	72.18	121.40	25.96	1112.17	0
4	A	45.44	78.19	28.18	644.99	97.3
	B	72.18	119.80	25.97	1111.74	0
5	A	62.14	107.15	26.85	925.73	107.15
	B	62.14	101.75	26.56	935.84	0
6	A	62.14	107.15	26.41	941.15	107.15
	B	62.14	100.06	26.55	936.19	0
7	A	62.14	107.15	25.87	960.80	107.15
	B	62.14	99.44	26.54	936.54	0
8	A	72.18	124.46	24.52	1177.48	124.46
	B	72.18	141.80	25.93	1113.46	0
9	A	72.18	124.46	23.63	1221.83	124.46
	B	72.18	112.66	25.91	1114.31	1000
Total	A	582.72	1000		8939.70	1000
	B	509.52	1000		9310.06	1000

At this point, we can state that the simplified model is useful because it provides a fast evaluation of the system without the need of detailed information. However, it is not appropriate for deducing the new structure. In fact, the simplified model was deduced by using the conventional desalination theory. This theory does not consider stream splitting, except for the recirculation stream. In others words, the original theory does

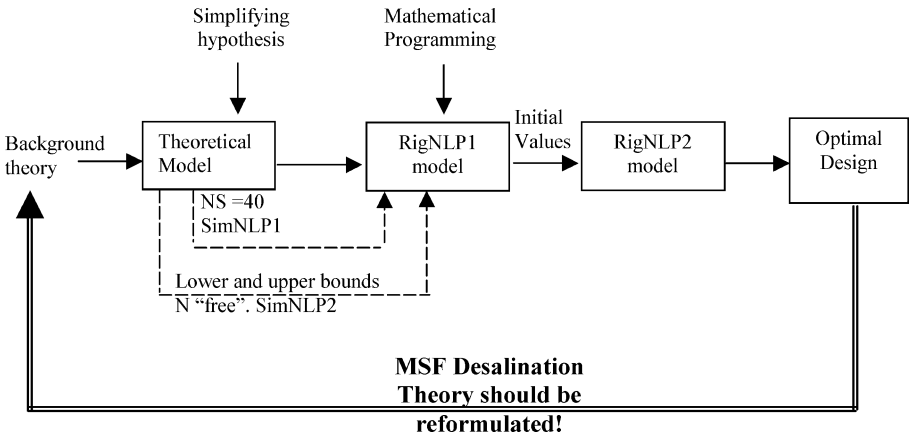

Figure 10. Suggested information retrofed according with the obtained results.

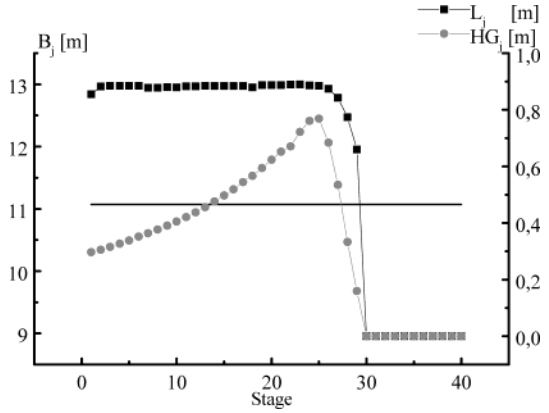

Figure 11. Length, gate height, and width distributions through the flashing chambers.

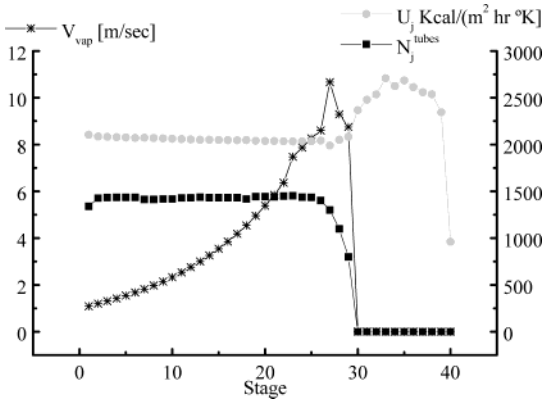

Figure 12. Tube number, heat-transfer coefficient, and vapor velocity distribution through the stages.

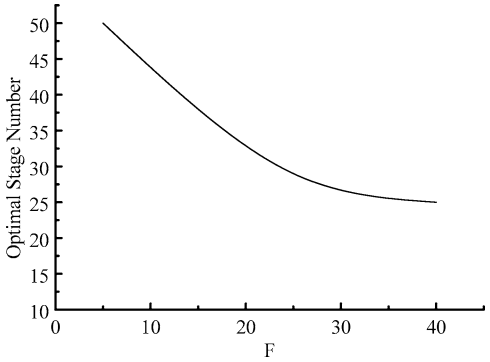

Figure 13. Optimal number of stages versus *F*.

not allow distillate extraction from the stages. It was also difficult to individualize reflashing operation relating heat exchange and distillate production. The tradeoff between distillate reflashing and distillate production was solved in the rigorous model. It is shown that the process is more efficient if some distillate is partially eliminated, avoiding reflashing.

A new structure for the MSF-M process resulted from the proposed NLP model based on a superstructure. According to the obtained results, the conventional theory of desalination should be modified. So, it is interesting to introduce a new simplified model to predict the "best" places in which the distillate extraction can be made (Figure 10).

Up to here, the main characteristics of the "new desaltor configuration", such as product extraction, recycle, and rejected streams allocation, were analyzed.

The length, the gate height, and the width stage distribution through the flashing chambers are shown in Figure 11.

The tubes number, the overall heat transfer, and the vapor velocities distribution through the flashing chamber are illustrated in Figure 12. It is clear that the solution is good enough to allow for a detailed design of the real process, that is, basic and detailed engineering.

Note that, in the proposed model, it is not necessary to consider integer and/or binary variables to achieve the optimal number of stages and other discrete decisions (feed and blowdown allocation, among others). In all cases, the variable values related to each stage, such as N_j^{tubes}, A_j^{tubes}, and V_j^p, among others, are equal to zero if stage j is deleted in the optimal solution. The same criterion is considered for the discrete decisions related to the allocations of the feed and blowdown streams. It is important to stress that, in all of the studied cases, the feed and blowdown streams are located only in one stage. For example, Figure 6 shows that the optimal feed flow rate is allocated in stage no. 29 while the blowdown stream is placed in stage no. 27.

5.2. Study Case 2. In this section, various examples will be solved in order to show the methodology robustness. Different values for the parameter *F* will be used. Also, a discussion about some computational difficulties is considered.

Table 4 shows the main resulting values achieved using the simplified model SimpNLP1 and the rigorous model RigNLP2 also indicating computational times. As can be seen, initial values predicted by the SimNLP1 model are "good values" in order to initialize the rigorous model variables (RigNLP1).

Table 4. Initial and Optimal Values of Study Cases for Example 2

F	model	Q^{Des} [Gcal/h]	tubes area [m^2]	stage area [m^2]	B [m]	L [m]	NS	TAC [$\times 10^6$ \$/year]	CPU time (s)
10	SimNLP1	69.88	42 880	1585	5.32	1.62	40[a]	1.029	0.391
	RigNLP2	73.71	44 080	1046	12.34	0.74	36	1.147	211.320
25	SimNLP1	75.43	38 690	1500	4.87	1.53	40[a]	1.213	0.332
	RigNLP2	80.38	41 480	867	12.06	0.80	29	1.251	320.182
40	SimNLP1	79.04	36 400	1369	4.21	1.67	40[a]	1.307	0.281
	RigNLP2	85.13	41 060	738	10.06	0.95	25	1.337	380.910

[a] Fixed value.

Figure 13 shows the influence of factor F on the optimal number of stages (NS). The optimal number of stages decreases considerably in the range $10 \le F \le 20$. For values higher than 20, the optimal NS decreases asymptotically to NS = 25.

All achieved solutions preserve the characteristics analyzed in study case 1. Again distillate extraction is distributed, the blowdown stream is not located at the last stage, and the total recycle flow rate is distributed along the last stages. Nevertheless, stage locations where these characteristics occur vary according to each problem. For example, for $F = 10$, 25, and 40, the stages in which the distillate extraction begins are 25, 22, and 18, respectively.

Finally, it is important to note that the previous study cases and many others not presented here were solved without using the preprocessing phase. In some cases, convergence problems appeared and the solutions could not be reached. The resulting difficulties were infeasible solutions, a large number of function evaluation errors, and large values for derivate Jacobian elements. In other cases, local solutions exhibiting poor objective values as well as a bad/wrong tube distribution, heat-transfer area, and distillate production along the stages were obtained.

6. Conclusions

A systematic and robust methodology for the optimal design of MSF evaporation systems has been presented.

The methodology uses the solution obtained by a simplified model to determine the initial values and bounds to solve the rigorous model easily. These values are determined automatically without external information. The main advantages of using simplified models are (a) there is a fast evaluation of the system with no need of detailed information, (b) they can be easily solved without convergence problems, and (c) bounds and initial values for solving the rigorous model are obtained.

In this paper, the superstructure for the MSF-M presented was modeled and successfully solved as a NLP problem. A new configuration for the MSF-M system resulted. This new structure differs from the conventional structure because in the former distillate extraction is considered and the blowdown brine stream is not allocated in the last stage. Based on these results, the classical desalination theory should be reformulated. This aspect will be approached in a future work.

Acknowledgment

We gratefully acknowledge Consejo Nacional de Investigaciones Científicas y Técnicas (CONICET), Universidad Nacional del Litoral (UNL), Agencia Nacional de Promoción de Ciencia y Técnica Argentina (ANPCyT), and International Center for Water and Energy Systems, ABU DHABI (ICWES), of the United Arab Emirates for their financial support.

Appendix 1.

Property Correlations.

For the water enthalpy [kcal/kg]

$$H_{liq} = [5415.943542(T - T_{Ref}) - 3.771131883(T^2 - T_{Ref}{}^2) + 0.00382052(T^3 - T_{Ref}{}^3)]\frac{10^{-3}}{4.1868}$$

For the latent heat of evaporation [kcal/kg]

$$\lambda_{Vap} = \frac{2589.583 + 0.9156T - 0.0048343T^2}{4.1868}$$

For the vapor enthalpy [kcal/kg]

$$H_{Vap} = H_{liq} + \lambda_{Vap}$$

For the solid enthalpy [kcal/kg]

$$H_{Solid} = \left[10.79(T - T_{Ref}) + \frac{0.00420}{2}(T^2 - T_{Ref}{}^2)\right]\frac{1}{70}$$

For the BPE [K] (Friedrich and Hafford, 1971)

$$BPE = (\sum_{i=0}^{2} a_i m^i)\frac{m}{a_3}$$

where

$$a_0 = \frac{565.757}{T} - 9.81559 + 1.54739 \ln(T)$$

$$a_1 = \frac{-337.178}{T} + 6.41981 - 0.922753 \ln(T)$$

$$a_2 = \frac{32.681}{T} - 0.55368 + 0.079022 \ln(T)$$

$$a_3 = \frac{266919.6}{T^2} - \frac{379.669}{T} + 0.334169$$

$$m = 19.819\frac{X}{1 - X}$$

For the overall heat-transfer coefficient [BTU/(h·ft^2·°F)][8]

$$U0 = \frac{U}{1 + UFF}$$

where

$$U = \frac{1}{z + y}$$

$$y = \frac{(\mathrm{vb} \times \mathrm{Di})^{0.2}}{(160 + 1.92\mathrm{Tb})\mathrm{vb}}$$

$$z = \sum_{i=0}^{4} a_i \mathrm{Tc}^i$$

where $a_0 = 0.102\,476\,8 \times 10^{-2}$, $a_1 = -0.747\,393\,9 \times 10^{-5}$, $a_2 = 0.999\,077 \times 10^{-7}$, $a_3 = -0.430\,046 \times 10^{-9}$, and $a_4 = 0.620\,674\,4 \times 10^{-12}$. z is the sum of the vapor-side resistances, y is the brine-side film resistance, Tc is the saturation temperature [°F], Tb is the brine temperature at the exit [°F], vb is the linear velocity of brine [ft/s], and Di is the inside diameter tube [in.]. Finally, the fouling factor FF [(h·ft²·°F/BTU] is considered as $8.544\,39 \times 10^{-4}$.

For the NEA [K] (there are several empirical correlations developed), we adopted for our model the correlations developed for Oak Ridge National Laboratory (ORNL):

$$\mathrm{NEA}_{10} = (0.9784)^{T_0}(15.7378)^{H}(1.377)^{W\times 10^{-6}}$$

$$\mathrm{NEA} = \left[\frac{\mathrm{NEA}_{10}}{0.5\Delta T_s + \mathrm{NEA}_{10}}\right]^{0.3281L}(0.5\Delta T_s + \mathrm{NEA}_{10})$$

where ΔT_s is the flashing range, W is the mass flow rate of the recirculated brine per unit of chamber width, and H is the brine level inside the flashing chamber.

Appendix II

In this appendix, the simplified model used on the preprocessing phase is presented. For more details, see ref 13.

Heat consumption (Q^{Des}):

$$Q^{\mathrm{Des}} = FC_p\Delta t \qquad \text{(A.II.1)}$$

$$\Delta t = \Delta t_f + \Delta t_e + \mathrm{BPE} \qquad \text{(A.II.2)}$$

where Δt_f, Δt_e, and BPE are temperature drop for the flashing operation, effective driving force for the heat-transfer operation, and boiling point elevation, respectively.

Total heat-transfer area A_t[13]

$$A_t = (FC_p/U)\mathrm{NS}\ \ln[(\Delta t - \mathrm{EPE})/\Delta t_e]^{(T_{\max}-\Delta t-T_o)/\Delta t_f} \qquad \text{(A.II.3)}$$

$$\mathrm{NS}\Delta t_f = T_{\max} - \Delta t - T_0 \qquad \text{(A.II.4)}$$

where NS is the number of stages and T_{Max} and T_0 are the top brine and seawater temperatures, respectively.

Total production of distillate (Prod)

$$\mathrm{Prod} = F\left[1 - \left(1 - \frac{C_{p,m}\Delta t_f}{\lambda}\right)^{\mathrm{NS}}\right] \qquad \text{(A.II.5)}$$

Relation among the heat-transfer area (A_t) with the number of tubes (N_t) and the chamber width (B)

$$A_t = \pi \mathrm{TD}BN_t\mathrm{NS} \qquad \text{(A.II.6)}$$

Chamber height

$$\mathrm{HS} \cong 2\mathrm{LB} + D_S \qquad \text{(A.II.7)}$$

Relation between the number of rows of tubes in the vertical direction (N) and the number of tubes N_t

$$N = 0.481\sqrt{N_t} \qquad \text{(A.II.8)}$$

Relation among the shell diameter (D_S), number of rows of tubes, and pitch P_t[4]

$$D_S = NP_t\sqrt{2} \qquad \text{(A.II.9)}$$

Length of the desaltor

$$\mathrm{LD} = \frac{\mathrm{Prod}}{BV_{\mathrm{vap}}\rho_{\mathrm{vap}}} \qquad \text{(A.II.10)}$$

where V_{vap} and ρ_{vap} are the velocity and density of the vapor, respectively

The following constraint must be satisfied:

$$\mathrm{LD} = D_S\mathrm{NS} \qquad \text{(A.II.11)}$$

Total stage surface area

$$A_S = 2LB + 2HL + H_SB \qquad \text{(A.II.12)}$$

Constraints related to the brine recirculation

$$F = \mathrm{SW} + W_R \qquad \text{(A.II.13)}$$

$$F = \mathrm{Prod} + W_R + W_{\mathrm{blow-d}} \qquad \text{(A.II.14)}$$

$$W_R = RW_{\mathrm{blow-d}} \qquad \text{(A.II.15)}$$

$$FC_pT_F = W_RC_pT_{\mathrm{blow-d}} + \mathrm{SW}C_pT_0 \qquad \text{(A.II.16)}$$

where W_R, $W_{\mathrm{blow-d}}$, and SW are the flow-rate values corresponding to recirculated, blown-down brine, and seawater streams.

The economic objective function is

$$\mathrm{TAC} = \mathrm{Minimize}\lfloor \mathrm{CRF}C_A(A_t + FA_S) + C_QQ^{\mathrm{Des}}\rfloor$$

Literature Cited

(1) Grossmann, I. E.; Caballero, J. A.; Yeomans, H. Mathematical Programming Approaches to the Synthesis of Chemical Process Systems. *Korean J. Chem. Eng.* **1999**, *16* (4), 407.

(2) Sommariva, C.; Pinciroli, D.; Sciubba, E.; Lior, N. Innovative configurations for Multi Stage Flash Desalination Plant. *Int. Desalin. Assoc., San Diego Proc.* **1999**, *1*, 65.

(3) El-Dessouky, H.; Shaban, H.; Al-Ramadan, H. Steady-state analysis of multi-stage flash desalination process. *Desalin. J.* **1995**, *103*, 271.

(4) El-Dessouky, H.; Ettouney, H.; Al-Roumi, R. Multi-stage flash desalination: present and future outlook. *Chem. Eng. J.* **1999**, *73*, 173.

(5) Androulakis, I. P.; Maranas, C. D.; Floudas, C. A. αBB: a Global Optimization Method for General Constrained Nonconvex Problems. *J. Global Optim.* **1995**, *7*, 337.

(6) Drud, A. CONOPT: A system for large scale nonlinear optimization. *Reference manual for CONOPT Subroutine Library, 69p, ARKI consulting and development A/S, Bagsvaerd*; Denmark, 1996.

(7) El-Sayed, Y. M.; Silver, R. S. In *Fundamentals of Distillation in Principles of Desalination*, 2nd ed.; Spliegler, K. S., Laird, A., Eds.; Academic Press: New York, 1980; Part A.

(8) Griffin, W.; Keller, R. Report ORNLL-TM-1299, Nov 1965.

(9) Helal, A.; Medani, M.; Soliman, M.; Flower, J. A TDM Model for MSF Desalination Plants. *Comput. Chem. Eng.* **1971**, *10* (4), 327.

(10) Genthner, K.; Al-Gobaisi, D.; Wangnick, F. The next size generation of MSF Evaporators: 100,000 cu-m/day. *Int. Desalin. Assoc., Madrid Proc.* **1997**, *1*, 271.

(11) Brooke, A.; Kendrick, D.; Meeraus, A. *GAMS: A user's guide*; The Scientific Press: San Francisco, 1996.

(12) Linnhoff, B.; Flower, J. Synthesis of Heat Exchanger Networks I. Systematic Generation of Energy Optimal Networks. *AIChE J.* **1978**, *24*, 633.

(13) Scenna, N. J. Synthesis of Thermal Desalination Processes. Ph.D. Thesis, Universidad Nacional del Litoral, Santa Fe, Argentina, 1987.

(14) Marcovecchio, M.; Mussati, S. Aplicación de Método de Optimización Global a un modelo de Evaporador Flash Múltiple Etapa. X Jornadas de Jóvenes investigadores de la Asociación de Universidades del Grupo Montevideo (AUGM), Florianópolis, Santa Catarina, Brazil.

(15) Mussati, S.; Aguirre, P.; Scenna, N. Synthesis and Optimization of Dual Purpose Thermal Desalination Plants. *Integrated Power and Desalination Plants. DAR Water Science and Technology*; PVT. Ltd. EOLSS Publisher Co. Ltd.: Oxford, U.K., 2002.

Received for review April 29, 2002
Revised manuscript received April 22, 2003
Accepted July 11, 2003

IE020318V